

SPACE-TIME WAVEFORM RELAXATION MULTIGRID FOR NAVIER-STOKES

JAMES JACKAMAN AND SCOTT MACLACHLAN

ABSTRACT. Space-time finite-element discretizations are well-developed in many areas of science and engineering, but much work remains within the development of specialized solvers for the resulting linear and nonlinear systems. In this work, we consider the all-at-once solution of the discretized Navier-Stokes equations over a space-time domain using waveform relaxation multigrid methods. In particular, we show how to extend the efficient spatial multigrid relaxation methods from [37] to a waveform relaxation method, and demonstrate the efficiency of the resulting monolithic Newton-Krylov-multigrid solver. Numerical results demonstrate the scalability of the solver for varying discretization order and physical parameters.

1. INTRODUCTION

High-fidelity computer simulation of fluid flow has been a common target in scientific computing since the 1960's [8, 22]. As both high-performance computing platforms and simulation technology have advanced, computational fluid dynamics has persisted as a driving application, seeking higher-fidelity models (e.g., by using pressure-robust finite-element methods [28]) and better use of highly parallel computing platforms (such as via GPU computing [16]). On modern manycore HPC systems, however, it is easy to reach saturation with spatial parallelism alone, where wallclock time to solution plateaus as increased communication costs outweigh any speedups gained by increasing core counts. Recent studies suggest this occurs for problem sizes below $\mathcal{O}(10,000)$ degrees of freedom per processor on many modern machines [34].

One way to achieve better performance in the strong scaling limit is the use of time-parallel algorithms (cf. [17]) to increase the number of degrees of freedom in concurrent computation. Recent years have seen the development of several families of time-parallel algorithms for numerical integration of PDEs, including Parareal [31], multigrid reduction-in-time (MGRIT) [13], ParaDIAG [18], waveform relaxation (both Schwarz and multigrid approaches) [4, 30, 32], and others. A common critique, however, is that these algorithms are often only demonstrated on simple discretizations of simple diffusive problems, and that their performance often suffers on more complex models (particularly hyperbolic PDEs) without substantial additional insights or costly stages in the algorithmic development [9, 10].

The focus of this manuscript is the development of multigrid waveform relaxation techniques for the Navier-Stokes equations, modeling time-dependent incompressible fluid flow. Waveform relaxation methods were first proposed in the 1980's for circuit simulation [30]. Their adaptation as a relaxation scheme for space-time multigrid methods was studied extensively in the 1990's, following the first work by Lubich and Ostermann [32]. Much of this work has focused on methods for the heat equation and similar scalar parabolic model problems [25–27, 39–41]. To our knowledge, the only previous application of multigrid waveform relaxation to the Navier-Stokes equations is the work of Oosterlee and Wesseling [35], but this work is limited to a low-order finite-volume discretization and BDF(2) time discretization. In particular, since higher-order BDF methods are not A-stable [20], extensions of this approach to higher-order discretizations are not immediately apparent. Furthermore, the multigrid method in [35] is based on a line relaxation strategy that is appropriate to the curvilinear coordinates used therein, but not needed for the simpler setting of Cartesian grids considered here.

The main contribution of this work is the extension of efficient spatial relaxation schemes for finite-element discretizations of the Poisson and time-steady Navier-Stokes equations to waveform relaxation schemes for space-time finite-element discretizations. We use standard continuous Lagrange finite-element methods for the spatial discretization of the heat equation, focusing on polynomial degrees from 1 to 3, and making

Date: July 22, 2024.

This work was partially supported by an NSERC Discovery Grant (SM) and the European Union's Horizon 2020 research and innovation program under the Marie Skłodowska-Curie grant agreement No 101108679 (JJ).

use of patch-based relaxation to obtain convergence rates that are independent of polynomial order. For Navier-Stokes, we use Taylor-Hood elements of both lowest and second-lowest order ($\mathbb{P}_2\text{-}\mathbb{P}_1$ and $\mathbb{P}_3\text{-}\mathbb{P}_2$), and demonstrate that the spatial relaxation proposed in [37] also extends to an effective waveform relaxation scheme. In both cases, we couple spatial semidiscretization with discontinuous-Galerkin timestepping, leading to space-time finite-element discretizations on prismatic grids. We demonstrate that the resulting Newton-Krylov-multigrid solver is highly efficient across a range of discretization orders and grid sizes, for two standard model problems.

The remainder of this paper is structured as follows. In section 2, we review the space-time finite-element formulation considered here. The waveform relaxation multigrid algorithm is detailed in section 3. Numerical results for both the heat equation and the Navier-Stokes equations are presented in section 4. Discussion and concluding remarks follow in section 5.

2. SPACE-TIME FINITE ELEMENT DISCRETIZATIONS

Throughout this work, we utilize space-time discretizations that, at their core, rely on a tensor-product structure separating the treatment of spatial and temporal domains. We make this choice as the PDEs under consideration possess fundamentally different dynamics in space and time. As such, we make use of tensor-product finite-element spaces and, for clarity, we expose our temporal and spatial discretizations independently. Before proceeding, we note that mixed space-time elements have proven successful when developing adaptive strategies [33] and are also well developed [23, 38, 42].

Here we consider upwind discontinuous Galerkin temporal elements, see [12]. This temporal discretization can be applied to any initial value problem (after reformulating it as a first-order-in-time system), so we consider the following: Let $\mathbf{y} \in [H^1([0, T], \mathcal{H}(\Omega))]^d$ where $d \in \mathbb{Z}^+$, $t \in [0, T]$ and $\mathbf{x} \in \Omega \subset \mathbb{R}^2$ and $\mathcal{H}(\Omega)$ represents an appropriate spatial Hilbert space. We first consider (evolutionary) PDEs of the type

$$\mathbf{y}_t + \mathcal{L}\mathbf{y} = 0 \quad \mathbf{y}(0, \mathbf{x}) = \mathbf{y}_0(\mathbf{x}), \quad (2.1)$$

subject to appropriate spatial boundary conditions, where \mathcal{L} is an infinite dimensional (nonlinear) differential operator and $\mathbf{y}_0 \in (\mathcal{H}(\Omega))^d$ is some given initial condition. Indeed, for any problem of this form, we can discretize temporally in a unified manner.

Definition 2.1 (Discontinuous Galerkin notation). Through partitioning our time interval into N sub-intervals $0 = t_0 < t_1 < \dots < t_N = T$, which we write as $I_n := (t_n, t_{n+1})$ for $0 \leq n < N$, we may define the discontinuous finite-element space of degree q as

$$\mathbb{V}_q([0, T], \mathcal{H}(\Omega)) = \left\{ Y \in L^2([0, T], \mathcal{H}(\Omega)) : Y|_{I_n} \in \mathbb{P}_q(I_n, \mathcal{H}(\Omega)), \text{ for } n = 0, \dots, N-1 \right\}, \quad (2.2)$$

where $\mathbb{P}_q(I_n, \mathcal{H}(\Omega))$ represents the space of degree q polynomials on I_n temporally (and functions in $\mathcal{H}(\Omega)$ spatially). We observe that this function space does not prescribe values at the temporal nodes t_n , which leads us to introduce the shorthand notations

$$\mathbf{Y}_n^+ := \lim_{t \nearrow t_n} \mathbf{Y}(t, \mathbf{x}) \quad \text{and} \quad \mathbf{Y}_n^- := \lim_{t \searrow t_n} \mathbf{Y}(t, \mathbf{x}). \quad (2.3)$$

For convenience, we further introduce the jump of a solution about a point t_n as $[[\mathbf{Y}_n]] := \mathbf{Y}_n^+ - \mathbf{Y}_n^-$.

Definition 2.2 (Temporal discretisation). Let \mathbf{y} solve (2.1), then our finite element approximation is given by seeking $\mathbf{Y}(\cdot, \mathbf{x}) \in [\mathbb{V}_q([0, T], \mathcal{H}(\Omega))]^d$ such that

$$\sum_{n=0}^{N-1} \int_{I_n} (\mathbf{Y}_t + \mathcal{L}\mathbf{Y}) \cdot \boldsymbol{\phi} dt + \sum_{n=0}^{N-1} [[\mathbf{Y}_n]] \cdot \boldsymbol{\phi}_n^+ = 0 \quad \forall \boldsymbol{\phi} \in [\mathbb{V}_q([0, T], \mathcal{H}(\Omega))]^d, \quad (2.4)$$

where we define $\mathbf{Y}_0^- := \mathbf{Y}_0 = \mathbf{y}_0(\mathbf{x})$ to be our initial condition in time.

Remark 2.3 (Efficient implementation in time). Typically, when exploiting a finite-element method in time of the form (2.4), one localizes the approximation to a single element and solves in a timestepping fashion. In this work, we primarily focus on solving *globally* in time, motivated by the temporal parallelism of the waveform relaxation multigrid method. We compare against a more typical timestepping implementation of the method in section 4.

Remark 2.4 (Conforming temporal discretisation). We note that for problems of the form (2.1), it is natural to seek $\mathbf{y} \in [H^1([0, T], \mathcal{H}(\Omega))]^d$ such that

$$\int_0^T (\mathbf{y}_t + \mathcal{L}\mathbf{y}) \phi \, dt = 0 \quad \forall \phi \in [L^2([0, T], \mathcal{H}(\Omega))]^d, \quad (2.5)$$

as this choice of (temporal) function spaces allows for the conditions of Lax-Milgram to be met, utilizing the fact that $\mathbf{y}_t \in [L^2([0, T], \mathcal{H}(\Omega))]^d$. To accurately discretize the temporal dynamics, this formulation allows use of continuous Lagrange elements of degree q for $\mathbf{Y}(\cdot, \mathbf{x})$ tested against discontinuous Lagrange elements of degree $q - 1$. However, the conforming nature in time restricts the ability to adapt in space-time so, in practice, the non-conforming upwind discontinuous Galerkin approximation (2.4) is often used. We note that this approximation adds numerical dissipation, the amount of which decreases as we increase the order of the method [12].

We will now proceed to discuss the problems under consideration and their spatial discretization. Throughout, we exploit the spatial L^2 inner product

$$\langle \mathbf{u}, \mathbf{v} \rangle := \int_{\Omega} \text{tr}(\mathbf{u}^T \mathbf{v}) \, d\mathbf{x}. \quad (2.6)$$

In the sequel, we shall abuse notation by allowing (2.6) to contract tensors to scalars (through the trace inner product).

We shall apply the algorithm developed in this work to two PDEs, namely the two-dimensional heat equation and incompressible Navier-Stokes equations. While both the examples below are presented without external forcing, such terms are easily added to the resulting weak forms and discretizations.

Definition 2.5 (Heat equation). Let $u = u(t, \mathbf{x}) \in H^1([0, T], H^2(\Omega))$ where $\Omega \subset \mathbb{R}^2$ solve the heat equation

$$u_t - \nabla^2 u = 0, \quad (2.7)$$

subject to initial data $u(0, \mathbf{x}) = u_0(\mathbf{x})$ and natural boundary conditions. Further let \mathcal{T}_h be a triangulation of the polygonal spatial domain and $\mathbb{P}_k(\mathcal{T}_h) \subset H^1(\Omega)$ be the space of continuous Lagrange elements of degree k . Then, recalling notation from our temporal discretization (Definition 2.2), our full discretization is described by seeking $U \in \mathbb{V}_q([0, T], \mathbb{P}_k(\mathcal{T}_h))$ such that

$$\sum_{n=0}^{N-1} \int_{I_n} \langle U_t, \psi \rangle \, dt + \sum_{n=0}^{N-1} \llbracket U_n \rrbracket \psi_n^+ + \int_0^T \langle \nabla U, \nabla \psi \rangle \, dt = 0 \quad \forall \psi \in \mathbb{V}_q([0, T], \mathbb{P}_k(\mathcal{T}_h)), \quad (2.8)$$

where we define $U_0^- := u_0(\mathbf{x})$ to be our initial condition.

Definition 2.6 (Navier-Stokes equations). Let $\mathbf{u} = \mathbf{u}(t, \mathbf{x}) \in [H^1([0, T], H^2(\Omega))]^2$ and $\phi = \phi(t, \mathbf{x}) \in L^2([0, T], H^1(\Omega))$ where $\Omega \subset \mathbb{R}^2$ is some bounded spatial domain subject to appropriate boundary conditions. We consider the incompressible fluid model

$$\begin{aligned} \mathbf{u}_t + R\mathbf{u} \cdot \nabla \mathbf{u} + \nabla \phi - \nabla^2 \mathbf{u} &= 0 \\ \nabla \cdot \mathbf{u} &= 0, \end{aligned} \quad (2.9)$$

where R is the Reynolds number. We discretize spatially with Taylor-Hood elements, i.e., we seek $\mathbf{U} \in [\mathbb{V}_q([0, T], \mathbb{P}_{k+1}(\Omega))]^2$ and $\Phi \in \mathbb{V}_q([0, T], \mathbb{P}_k(\Omega))$ such that

$$\begin{aligned} \sum_{n=0}^{N-1} \int_{I_n} \langle \mathbf{U}_t, \boldsymbol{\psi} \rangle \, dt + \sum_{n=0}^{N-1} \llbracket \mathbf{U}_n \rrbracket \cdot \boldsymbol{\psi}_n^+ \\ + \int_0^T \langle R\mathbf{U} \cdot \nabla \mathbf{U}, \boldsymbol{\psi} \rangle + \langle \Phi, \nabla \cdot \boldsymbol{\psi} \rangle + \langle \nabla \mathbf{U}, \nabla \boldsymbol{\psi} \rangle \, dt = 0 \quad \forall \boldsymbol{\psi} \in [\mathbb{V}_q([0, T], \mathbb{P}_{k+1}(\Omega))]^2 \end{aligned} \quad (2.10)$$

$$\int_0^T \langle \nabla \cdot \mathbf{U}, \chi \rangle \, dt = 0 \quad \forall \chi \in \mathbb{V}_q([0, T], \mathbb{P}_k(\Omega)).$$

We note that the Navier-Stokes equations do not precisely fall into the framework described above, since they form a system of differential algebraic equations (DAEs), but the discretization above arises from consistently applying the space-time discretization framework in this setting. We shall consider two test cases for (2.10) in this work, both posed on domain $\Omega = [0, 1] \times [0, 1]$.

Definition 2.7 (Chorin test problem [8]). Fixing zero Dirichlet boundary conditions on the normal component of \mathbf{u} , we obtain the Chorin test problem [8] which has exact solution given by velocity

$$\mathbf{u}(t, \mathbf{x}) = \begin{pmatrix} -\cos(\pi x_1) \sin(\pi x_2) \\ \sin(\pi x_1) \cos(\pi x_2) \end{pmatrix} e^{-2\pi^2 t}, \quad (2.11a)$$

with corresponding pressure

$$\phi = R \frac{\pi}{4} (\cos(2\pi x_1) + \cos(2\pi x_2)) e^{-4\pi^2 t}. \quad (2.11b)$$

Remark 2.8 (Dependence on Reynolds number). Typical solutions of the Navier-Stokes equations are expected to exhibit strong dependence on the Reynolds number, including steeping slopes of the velocity near domain boundaries where no-slip or no-flow boundary conditions are applied. In contrast to this, the velocity solution to the Chorin test problem is independent of the Reynolds number, and the pressure solution only shows linear dependence. Thus, while having an analytical solution for this test problem allows us to verify accuracy of our computed solutions, it does not provide a realistic test of solvers for Navier-Stokes in typical situations. For this reason, we also consider the case of a lid-driven cavity, which demonstrates much more complex dynamics.

Definition 2.9 (Lid-driven cavity [5]). We fix zero velocity boundary conditions on both components of the velocity on the bottom, left and right boundaries,

$$\mathbf{u}|_{\Gamma_1} = \begin{pmatrix} 0 \\ 0 \end{pmatrix}, \quad (2.12)$$

and fix a velocity of

$$\mathbf{u}|_{\Gamma_2} = \begin{pmatrix} 1 \\ 0 \end{pmatrix} \quad (2.13)$$

on the top boundary. The test case is then initialized with zero velocity \mathbf{u} and pressure ϕ . Such an initialization lends itself, over time, to the well studied steady laminar solution, see, for example, [5, 7].

3. WAVEFORM RELAXATION MULTIGRID

Classical multigrid methods make use of two complementary processes to damp errors in an approximation to the solution of a discretized system of differential equations, known as relaxation and coarse-grid correction. In the setting of a simple elliptic (time-steady) PDE, relaxation is used to efficiently damp high-frequency errors in an approximation, leaving a smooth error, which can be effectively approximated by solution of a restricted problem on a coarser spatial grid. While multigrid theory and practice were first developed for elliptic PDEs, questions on how to extend these approaches to time-dependent problems arose in the early 1980's [19]. We note that applying spatial multigrid to a single timestep of a fully discretized time-dependent PDE is quite natural, particularly when implicit Euler or Crank-Nicolson type discretizations are used, and was considered even earlier in the development of multigrid [6]. Instead, we are focusing on cases that solve the full space-time discretization over multiple timesteps concurrently, using relaxation and coarse-grid correction processes defined over all space-time grid points, and not just on a single time-line.

As noted above, the dynamic behavior of solutions to many time-dependent PDEs is dramatically different in the temporal direction than in the spatial direction. As such, even the earliest works on multigrid for space-time problems typically considered coarsening only in the spatial direction, commonly known as semi-coarsening, an approach also considered for other problems with very anisotropic behavior. While Hackbusch's original approach simply used the space-time analogues of Jacobi or Gauss-Seidel point relaxation techniques, Lubich and Oostermann quickly proposed the use of so-called waveform relaxation [30] techniques as relaxation methods for space-time multigrid problems [32]. This approach was extensively studied and developed in the 1990's, particularly by Vandewalle and collaborators [25–27, 39–41].

Here we consider a standard geometric multigrid interpretation of waveform relaxation multigrid. Given a hierarchy of spatial meshes, $\{\mathcal{T}_H, \mathcal{T}_{H/2}, \dots, \mathcal{T}_h\}$, and fixed temporal mesh $0 = t_0 < t_1 < \dots < t_N = T$,

we create a hierarchy of space-time grids as $\{t_n\}_{n=0}^N \otimes \mathcal{T}_H, \{t_n\}_{n=0}^N \otimes \mathcal{T}_{H/2}, \dots, \{t_n\}_{n=0}^N \otimes \mathcal{T}_h$, where we use Kronecker-product notation to denote the space-time mesh formed by a tensor product of a temporal mesh with a spatial one. We use standard geometric multigrid V-cycles as preconditioners for FGMRES, where we use FGMRES not for its flexibility (we use stationary V-cycles), but because it explicitly stores the preconditioned Arnoldi vectors and, thus, can reassemble the final solution without the additional application of the preconditioner needed in classical right-preconditioned GMRES. In all experiments, we use V(2,2) cycles, where both the pre- and post-relaxation sweeps are accelerated by a Chebyshev polynomial. To determine the interval to define the Chebyshev polynomial, we use 50 steps of relaxation-preconditioned GMRES to estimate the largest eigenvalue of the preconditioned system, λ , and choose the interval to be $[0.25\lambda, 1.05\lambda]$, where we choose the factor of 1/4 because we are coarsening by a factor of two in two spatial dimensions, and 1.05 to provide a safety factor, in case λ is an underestimate of the true largest eigenvalue. These choices essentially give optimal relaxation weights to reduce the errors associated with the upper 3/4 of the spectrum of the relaxation-preconditioned system (provided that λ is a good estimate of the largest eigenvalue of the relaxation-preconditioned system).

We now describe the grid-transfer operators and waveform relaxation variants that we use for the two model problems considered here. For the heat equation, we construct interpolation to space-time grid $\{t_n\}_{n=0}^N \otimes \mathcal{T}_h$ as $P = I \otimes P_h$, where I is an identity operator over the temporal mesh and P_h is the standard finite-element interpolation from grid $2h$ to grid h for the \mathbb{P}_k elements. This expression for interpolation assumes that the degrees of freedom are ordered consistently with the tensor-product mesh expressions above but, in practice, this need not be the case. For restriction from this grid, we use $R = P^T$. For relaxation for the heat equation, we use vertex-star relaxation [15] in the spatial domain, extended (in the usual style of waveform relaxation) to couple all degrees of freedom in space-time that reside in the spatial patch. Vertex-star patches are defined by taking each vertex in the mesh, identifying all edges and elements incident on the vertex, and then taking the set of DoFs associated with the vertex itself and those internal to the incident edges and elements. A sample such patch for \mathbb{P}_2 on a regular triangular mesh is shown at left of Figure 1. We note that such a spatial patch solve is known to lead to robust preconditioners for the Poisson equation (see, for example, [36]), so we expect to see robust performance for the heat equation using its waveform relaxation analogue.

For the Navier-Stokes equations, we require two generalizations to the components used for the heat equation. First, in usual (spatial) monolithic multigrid style, the spatial interpolation operator P_h is now block diagonal,

$$P_h = \begin{bmatrix} P_{\mathbf{u}} & 0 \\ 0 & P_{\phi} \end{bmatrix}, \quad (3.1)$$

where $P_{\mathbf{u}}$ is the appropriate (spatial) finite-element interpolation for the vector velocity space and P_{ϕ} is the appropriate (spatial) finite-element interpolation for the scalar pressure space. Again, we use space-time interpolation operator $P = I \otimes P_h$ and restriction operator $R = P^T$, assuming compatible ordering of the discrete degrees of freedom. For relaxation, we use the waveform relaxation analogue of the Vanka+star relaxation recently proposed in [37]. Here, we define spatial patches around each vertex in the mesh. Each patch contains all velocity degrees of freedom in the closure of the star of the vertex, which includes all velocity DoFs at the vertex itself, on the edges and elements incident on the vertex, and on edges and vertices directly adjacent to these edges and elements. Along with these, we include all pressure DoFs on the vertex star. For a Taylor-Hood discretization with a \mathbb{P}_2 velocity space and \mathbb{P}_1 pressure space, this is the usual Vanka patch, but this patch has been observed to yield convergence that is robust in polynomial order for higher-order Taylor-Hood discretizations of time-independent problems. A sample patch for the case of a $(\mathbb{P}_3)^2$ - \mathbb{P}_2 discretization is shown at right of Figure 1.

We implement these relaxation schemes in Firedrake [21], taking advantage of the “extruded mesh” functionality [3]. To do so, we define a spatial mesh hierarchy by defining the coarsest grid, \mathcal{T}_H , and uniformly refining it a given number of times. Then, we create a hierarchy of space-time grids as an extruded mesh hierarchy with a fixed (uniform) temporal grid at each level. This allows us to specify space-time function spaces for the discretization by defining spatial and temporal finite elements, on triangles and intervals, respectively, then defining tensor product elements, and defining function spaces to use these tensor-product elements over the space-time grids. The extruded mesh construction lets us easily construct

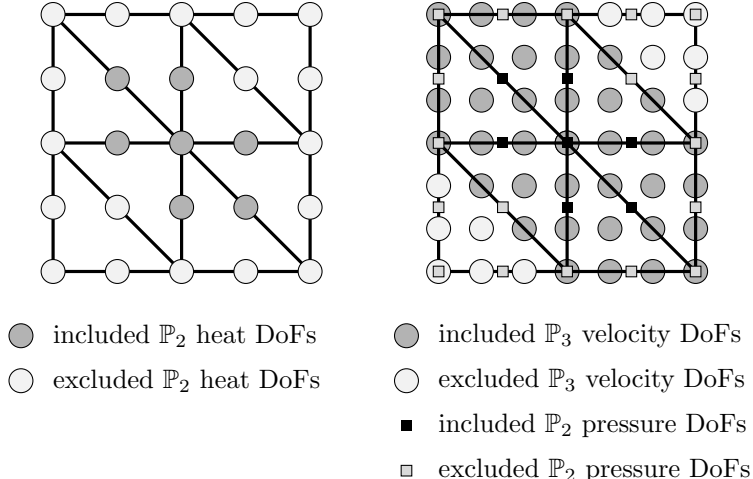


FIGURE 1. At left, a sample spatial vertex-star patch used for relaxation for the \mathbb{P}_2 elements for the heat equation. At right, a sample Vanka+star patch for the $(\mathbb{P}_3)^2$ - \mathbb{P}_2 discretization of the Navier-Stokes equations.

patches for waveform relaxation, as we can do this using the PETSc DMPlex abstraction to manage the construction [29]. As extruded meshes are implemented in Firedrake, all space-time DoFs are assigned to spatial topological entities based on their spatial positioning on the grid, so that we can define patches for space-time extruded hierarchies in the same way as we do for spatial hierarchies, just by looping over the topological entities in the DMPlex structure.

4. NUMERICAL EXPERIMENTS

Our implementation can be found in [24], which utilizes the Firedrake and PETSc libraries [2, 21]. The specific versions of the Firedrake packages used are recorded here [43]. Throughout, we initialize our coarsest spatial mesh as a regular triangulation of the unit square domain, $\Omega = [0, 1]^2$, with 10 quadrilateral cells in both the x and y directions cut into 2 triangles each from bottom-right to top-left. This base spatial mesh is then uniformly refined \mathcal{M}_{ref} times, forming the hierarchy of spatial meshes. Temporally, we extrude each mesh in our hierarchy identically and uniformly, with N elements. Simulations are performed across 8 Xeon 2.4GHz CPU cores (unless otherwise stated) with a memory limit of 128GB per simulation. When a simulation cannot be run within the allocated memory, we represent this in our experiments by writing “OOM”.

4.1. Heat equation. Before applying the WRMG method detailed in §3 to the Navier-Stokes equations, we first apply it to the heat equation, as described in Definition 2.5 with initial condition $u_0(x) = \sin(\pi x) + \cos(2\pi y)$ and homogeneous Neumann BCs. Due to the rapid decay of solutions over time, we restrict our study to the time window $t \in [0, 0.02]$ and use $N = 20$ timesteps. Since this problem is linear, we solve it with WRMG-preconditioned FGMRES with a convergence tolerance requiring a reduction in the residual norm either by a relative factor of 10^{-6} or to below an absolute tolerance of 10^{-6} , and compare to the cost of solving the single (space-time) linear system once with an LU factorization. In all experiments reported below, all FGMRES-WRMG solves take only 3 iterations to reach this convergence tolerance except for the case of temporal degree 3 and spatial degree 2 with $\mathcal{M}_{\text{ref}} = 3$, which takes 4 iterations.

Table 1 presents some information about the discretization for various temporal and spatial degrees at $\mathcal{M}_{\text{ref}} = 3$, where the finest grid has $2 \times 80^2 = 12800$ spatial elements. At lowest order (0 in time and 1 in space), we see about 1.3×10^5 total DoFs, which makes sense for a problem with $81^2 = 6561$ spatial degrees of freedom and 20 time steps, giving 131 thousand total DoFs. For this problem, we see that there are about 20 nonzeros per row, corresponding to the 7-point spatial stencil for the stiffness and mass matrices coupled across 3 timesteps (since timestep n gets data from timestep $n - 1$ and gives data to timestep $n + 1$). As we increase the order in time, we see the number of DoFs grows linearly, while the number of nonzero entries in

TABLE 1. Total number of space-time degrees of freedom (left) and number of nonzero matrix entries (right) for the discretization of the heat equation at various spatial and temporal degrees with $\mathcal{M}_{\text{ref}} = 3$.

	Degrees of Freedom			Nonzero matrix entries		
3	5.2e5	2.1e6	4.6e6	4.2e7	2.7e8	9.1e8
2	3.9e5	1.6e6	3.5e6	2.4e7	1.5e8	5.1e8
1	2.6e5	1.0e6	2.3e6	1.1e7	6.9e7	2.3e8
0	1.3e5	5.2e5	1.2e6	2.6e6	1.7e7	5.9e7
time \ space	1	2	3	1	2	3

TABLE 2. Total computational time (in seconds) to solve the discretization of the heat equation at various spatial and temporal degrees with $\mathcal{M}_{\text{ref}} = 3$. At left, results for direct solution (LU factorization). At right, times for FGMRES-WRMG. Results shown as “OoM” denote that the solver ran out of memory.

	direct solver			FGMRES-WRMG		
3	28.1	226.2	OoM	6.0	34.3	103.2
2	14.3	108.8	OoM	4.0	23.2	65.8
1	6.8	45.6	113.2	3.0	8.2	34.9
0	2.7	13.7	40.1	2.2	4.1	9.5
time \ space	1	2	3	1	2	3

the matrix grows somewhat more quickly. As we increase the spatial order, we see quadratic growth in the number of DoFs and faster growth in the number of nonzeros in the matrix. Table 2 shows the corresponding times-to-solution, where we see somewhat sub-linear scaling in time-to-solution versus number of nonzero matrix entries using WRMG, with (for example) total time only increasing by 1.4 \times with spatial degree 1 and temporal degree going from 1 to 2, even those the number of DoFs in the system doubles, and the number of nonzeros increases by a factor of over 2. Notably, FGMRES-WRMG outperforms direct solution of the monolithic space-time system in every instance, including two of the highest-order cases where the direct solver runs out of memory.

Similar data for the heat equation at $\mathcal{M}_{\text{ref}} = 4$ is presented in Tables 3 and 4. As expected, the problem sizes and number of nonzero matrix entries reported in Table 3 are consistently approximately 4 times those in Table 1 (with slight variations due to rounding and the effects of boundary conditions). Notably, we see that WRMG is able to solve problems with up to 14 million discrete DoFs and up to 2 billion nonzero matrix entries within the allotted memory footprint, while solving the monolithic system with LU fails for problems with more than about 230 million nonzero matrix entries (and 4 million DoFs). Computational times in Table 4 show much more extreme scaling than in Table 2. At spatial degrees 1 and 2, FGMRES-WRMG now shows roughly linear scaling in the number of DoFs and/or number of nonzero matrix entries for the problem, while LU solution shows roughly quadratic scaling, with over 16 \times the computational time for time degree 3 and space degree 1 than for time degree 0 and space degree 1, even though the number of DoFs only increases by a factor of 4. This cost, however, closely mirrors the growth in the number of nonzeros in the matrix. Overall, we see substantial problems with the direct solver running out of memory, while this only occurs for the highest-order problem with FGMRES-WRMG.

TABLE 3. Total number of space-time degrees of freedom (left) and number of nonzero matrix entries (right) for the discretization of the heat equation at various spatial and temporal degrees with $\mathcal{M}_{\text{ref}} = 4$.

	Degrees of Freedom			Nonzero matrix entries		
3	2.1e6	8.2e6	OoM	1.7e8	1.1e9	OoM
2	1.6e6	6.2e6	1.4e7	9.4e7	6.2e8	2.0e9
1	1.0e6	4.1e6	9.3e6	4.2e7	2.7e8	9.1e8
0	5.2e5	2.1e6	4.6e6	1.0e7	6.8e7	2.3e8
time \ space	1	2	3	1	2	3

TABLE 4. Total computational time (in seconds) to solve the discretization of the heat equation at various spatial and temporal degrees with $\mathcal{M}_{\text{ref}} = 4$. At left, results for direct solution (LU factorization). At right, times for FGMRES-WRMG. Results shown as “OoM” denote that the solver ran out of memory.

	direct solver			FGMRES-WRMG		
3	198.1	OoM	OoM	16.6	270.7	OoM
2	102.7	OoM	OoM	10.9	167.3	607.8
1	38.8	OoM	OoM	7.1	110.1	300.5
0	11.2	69.0	211.28	4.4	51.6	120.4
time \ space	1	2	3	1	2	3

4.2. Navier-Stokes: Chorin test problem.

We now move on to consider the Chorin test problem for the Navier-Stokes equations, as described in Definition 2.7. Recall that this test problem is constructed with a known (manufactured) solution (see (2.11)), so we can measure the error in our computed solutions. Here, we choose to measure the space-time L^2 error in the velocity as a measure of the effectiveness of the solvers and discretizations. Since the Navier-Stokes equations are nonlinear, we use Newton’s method to solve the nonlinear problem, and then either a direct (LU) solver or WRMG-preconditioned FGMRES for the resulting linear solves. In both cases, we use stopping tolerances based on the norm of the nonlinear residual, requiring a relative reduction in the norm by a factor of 10^{-8} . When using the Newton-Krylov-multigrid approach, we use the Eisenstat-Walker stopping criteria for FGMRES to optimize performance, with looser linear solve convergence tolerance when we are far from solution [11]. We use the same mesh hierarchy as described above for the heat equation, and consider the time interval $t \in [0, 0.1]$, which we divide uniformly into 10, 20, and 40 temporal elements (N) in the experiments below. All results presented in this section are for the case of Reynolds number $R = 10$, but we recall Remark 2.8 and note that very similar results were seen for $R = \mathcal{O}(10^2)$.

Table 5 shows the space-time velocity error norms generated using the Newton-Krylov-multigrid solver as we vary the spatial and temporal finite-element orders (noting that we report the spatial order as the order of the pressure space, with the velocity space being one order higher), for various values of N , the number of timesteps. We note that these results are consistent with the hypothesis that the accuracy of this discretization is strongly controlled by time-stepping error. At temporal degree 0 and spatial degree 1, we see a clear scaling like $1/N$ in the reported errors, dropping to $1/N^2$ at temporal degree 1. With one outlier (at $N = 10$), the errors for spatial degree 2 are identical to those for spatial degree 1. Upon further investigation, we found that requiring a stricter stopping tolerance of a relative reduction in the norm of the nonlinear residual by a factor of 10^{-10} led to an error for $N = 10$, spatial degree 2 and temporal degree 0 that matches the 6.51×10^{-3} reported for $N = 10$, spatial degree 1 and temporal degree 0, computed with 5 Newton iterations and 13 total linear iterations in 98.2 seconds, only a slight increase on the time reported below in Table 6. Unfortunately, within the memory limitations of our computing platform, we

TABLE 5. $\mathcal{M}_{\text{ref}} = 3$ and $R = 10$: Space-time L^2 errors in velocity for the Chorin test problem for various temporal and spatial orders and numbers of timesteps, N , using the FGMRES-WRMG solver for the Newton linearizations. Results shown as “OoM” denote that the solver ran out of memory.

	N			N		
	10	20	40	10	20	40
1	1.77e-3	4.60e-5	1.18e-5	1.77e-3	OoM	OoM
0	6.51e-3	3.32e-3	1.70e-3	1.44e-3	3.32e-3	1.70e-3
time	1			2		
space						

TABLE 6. $\mathcal{M}_{\text{ref}} = 3$ and $R = 10$: Time-to-solution (in seconds) for the Chorin test problem for various temporal and spatial orders and numbers of timesteps, N , using the FGMRES-WRMG solver for the Newton linearizations. Results shown as “OoM” denote that the solver ran out of memory.

	N			N		
	10	20	40	10	20	40
1	101.2	209.1	441.7	339.5	OoM	OoM
0	31.0	63.9	126.2	91.7	186.9	387.5
time	1			2		
space						

TABLE 7. $\mathcal{M}_{\text{ref}} = 3$ and $R = 10$: Number of space-time DoFs for the Chorin test problem for various temporal and spatial orders and numbers of timesteps, N .

	N			N		
	10	20	40	10	20	40
1	1.2e6	2.3e6	4.7e6	2.8e6	OoM	OoM
0	5.8e5	1.2e6	2.3e6	1.4e6	2.8e6	5.7e6
time	1			2		
space						

were unable to run this problem at sufficiently high orders in time to balance the spatial discretization error for the smooth solution considered here.

Time-to-solution for the Newton-Krylov-multigrid solver is shown in Table 6. We do not include tables of iterations for this problem, because they are quite consistent. All converged runs shown in these tables took 5 Newton steps, and all took 7 total linear iterations, with the exception of $N = 10$ with temporal degree 0 and spatial degree 1, which took 8 linear iterations. Thus, the wall-clock time scaling is quite predictable, with linear dependence on N , and slightly worse than linear dependence on the number of DoFs, shown in Table 7, but slightly better than linear dependence on the number of nonzeros in the matrix, shown in Table 8.

For comparison, Table 9 shows time-to-solution for the same problems using Newton-LU as the solver. The most striking thing to notice is how few cases can be run in comparison to the Newton-Krylov-multigrid solver results above. Also quite clear is the more dramatic scaling of time-to-solution with N , with the run for $N = 20$ with spatial degree 1 and temporal degree 0 taking four times as long as with $N = 10$, in

TABLE 8. $\mathcal{M}_{\text{ref}} = 3$ and $R = 10$: Number of nonzero matrix entries for the Chorin test problem for various temporal and spatial orders and numbers of timesteps, N .

	N			N		
	10	20	40	10	20	40
1	1.9e8	4.0e8	8.1e8	7.2e8	OoM	OoM
0	4.8e7	1.0e8	2.0e8	1.8e8	3.7e8	7.6e8
time space	1			2		

TABLE 9. $\mathcal{M}_{\text{ref}} = 3$ and $R = 10$: Time-to-solution (in seconds) for the Chorin test problem for various temporal and spatial orders and numbers of timesteps, N , using a direct (LU) solver for the Newton linearizations. Results shown as “OoM” denote that the solver ran out of memory.

	N			N		
	10	20	40	10	20	40
1	175.2	OoM	OoM	OoM	OoM	OoM
0	35.8	160.0	OoM	113.0	OoM	OoM
time space	1			2		

contrast to the perfectly linear scaling with N observed for FGMRES-WRMG in Table 6. Similarly, the time-to-solution jumps by a factor of five when increasing from temporal degree 0 to 1, which is much more significant than for the FGMRES-WRMG case. We do not report the number of Newton iterations in this table, noting that 3 iterations were required for all four cases that produced results. Similarly, the accuracies of the computed velocities matched those in Table 5 for all cases except that of $N = 10$ with temporal degree 0 and spatial degree 2, where it matched the error for the stricter stopping tolerance discussed above.

4.3. Navier-Stokes: Lid-driven cavity. For our final test problem, we consider the lid-driven cavity problem for Reynolds numbers $R = 1, 10,$ and 100 . All solver parameters are chosen as in §4.2, and we consider the temporal domain $t \in [0, 0.02]$, subdivided into $N = 20$ temporal elements. We note that the number of DoFs and nonzero matrix entries for this system at $\mathcal{M}_{\text{ref}} = 3$ are the same as those reported for $N = 20$ in Tables 7 and 8, and those for $\mathcal{M}_{\text{ref}} = 2$ and $\mathcal{M}_{\text{ref}} = 4$ are simply one-fourth and four times the size, respectively, so we do not report them here.

We first demonstrate the effectiveness of our solvers in terms of the number of Newton steps to convergence and the total number of FGMRES-WRMG iterations required for those steps, as reported in Table 10. Here, we see there is some slight growth in the number of nonlinear and linear iterations with Reynolds number, but the growth is quite minor. In comparison, using direct solvers to solve the linear systems consistently requires 2 Newton iterations for $R = 1$, 3 Newton iterations for $R = 10$, and 4 Newton iterations for $R = 100$.

Times-to-solution for both solvers, using LU and FGMRES-WRMG to solve the Newton linearizations, are reported in Tables 11 and 12, respectively. From Table 11, we note the impact of the increasing numbers of Newton iterations to convergence, where the time-to-solution grows substantially with R . In contrast, times reported in Table 12 are roughly independent of the Reynolds number. We also note substantially improved times-to-solution when using the FGMRES-WRMG linear solver, which appears to scale roughly with the number of DoFs, in comparison to the substantially faster growth in time-to-solution using LU as the discretization is refined, shown in Table 11.

TABLE 10. Number of nonlinear and linear iterations needed for convergence for Newton’s method using FGMRES-WRMG as the linear solver for the lid-driven cavity problem for various temporal and spatial orders with varying Reynolds number, R , and \mathcal{M}_{ref} . Results shown as “OoM” denote that the solver ran out of memory.

		R			R		
		1	10	100	1	10	100
$\mathcal{M}_{\text{ref}} = 2$	1	4 (6)	4 (6)	5 (7)	5 (5)	5 (5)	5 (6)
	0	4 (6)	4 (6)	5 (7)	5 (5)	5 (5)	5 (6)
$\mathcal{M}_{\text{ref}} = 3$	1	4 (6)	4 (6)	5 (7)	OoM	OoM	OoM
	0	4 (6)	4 (6)	5 (7)	4 (5)	4 (5)	5 (6)
time / space		1			2		

TABLE 11. Time to solution (in seconds) needed for convergence for Newton’s method using direct linear solvers for the lid-driven cavity problem for various temporal and spatial orders with varying Reynolds number, R , and \mathcal{M}_{ref} . Results shown as “OoM” denote that the solver ran out of memory.

		R			R		
		1	10	100	1	10	100
$\mathcal{M}_{\text{ref}} = 2$	1	98.8	135.7	210.3	380.1	554.0	717.9
	0	18.7	28.3	35.2	66.0	95.2	124.2
$\mathcal{M}_{\text{ref}} = 3$	1	OoM	OoM	OoM	OoM	OoM	OoM
	0	121.1	174.0	213.4	OoM	OoM	OoM
time / space		1			2		

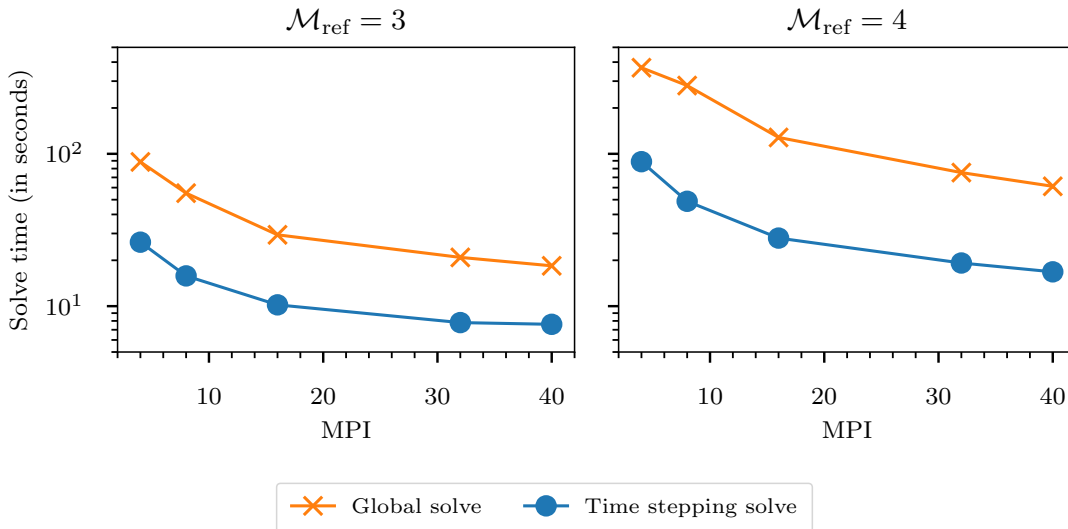
TABLE 12. Time to solution (in seconds) needed for convergence for Newton’s method using FGMRES-WRMG as linear solvers for the lid-driven cavity problem for various temporal and spatial orders with varying Reynolds number, R , and \mathcal{M}_{ref} . Results shown as “OoM” denote that the solver ran out of memory.

		R			R		
		1	10	100	1	10	100
$\mathcal{M}_{\text{ref}} = 2$	1	46.7	46.5	55.9	199.2	197.9	202.3
	0	16.1	15.6	18.1	48.9	48.9	49.1
$\mathcal{M}_{\text{ref}} = 3$	1	177.4	177.7	213.1	OoM	OoM	OoM
	0	55.0	54.9	64.3	155.2	155.0	184.7
time / space		1			2		

Finally, we consider a strong scaling experiment with increasing number of MPI ranks, comparing our monolithic Newton-Krylov-multigrid solver against a standard timestepping approach to solve the same problem using Newton’s method to solve each timestep sequentially, using FGMRES preconditioned by the corresponding spatial multigrid solver (constructed similarly to those in [1], solving for all temporal DoFs within a single timestep using a monolithic multigrid approach). We note that the timestepping approach results in a significantly smaller system to solve (with 1/20th the number of DoFs, in the example considered here) for each timestep, but one that must be solved 20 times to timestep to the same final solution time.

Figure 2 shows timing results for the problem with temporal degree 0 and spatial degree 1 at $\mathcal{M}_{\text{ref}} = 3$ and $\mathcal{M}_{\text{ref}} = 4$. Here, we see that the timestepping solver is consistently about 5 times faster than the monolithic solve using WRMG.

FIGURE 2. Time-to-solution (in seconds) for temporal degree 0 and spatial degree 1 for a simulation of the lid-driven cavity Navier-Stokes test case with $R = 10$ for differing numbers of MPI ranks. Here, we compare solving the global space-time system using WRMG as a preconditioner for GMRES against localizing the system to a single timestep and solving sequentially over the timesteps.



Clearly, in this regime (few timesteps in comparison to the spatial mesh sizes), the monolithic Newton-Krylov-multigrid approach is not competitive with the timestepping approach. We note, however, that there are advantages for the monolithic space-time approach that we have not yet exploited in the results presented here, due to limitations on our testing platform. Primarily, the WRMG approach is able to exploit finer-grained parallelism by using cyclic-reduction (or similar parallel direct solvers) to make effective use of more parallel cores by decomposing the space-time solves within the waveform relaxation [14]. Thus, on a system where many more cores are available, we can use a “two-level” approach to parallelism for WRMG, first decomposing the spatial grid to a sensible parallel distribution, then decomposing the temporal grid in a space-time parallel manner (that is not currently supported by Firedrake). This also would allow us to make use of a common feature of modern parallel architectures, where the amount of memory available scales with the number of cores, supporting the higher memory footprint of monolithic space-time solvers. We leave implementing and investigating this option for future work.

5. CONCLUSION

In this paper, we have demonstrated that the effective spatial multigrid relaxation scheme proposed for the Taylor-Hood discretization of the Navier-Stokes equations in [37] extends to an efficient monolithic Newton-Krylov-multigrid solver for space-time finite-element discretizations. The solver is shown to be effective for two-dimensional flow problems, both for the simple Chorin vortex problem and the more complicated lid-driven cavity problem. A notable feature of the solver is that the use of the Eisenstat-Walker stopping criterion for Newton’s method enables solution times that are much more insensitive to Reynold’s number than when using LU solvers, which suffer when the number of Newton steps needed to convergence increases.

Due to a software limitation in Firedrake, we are unable to extend the method to three-dimensional flows at this time. Overcoming this limitation is a key step in future work. Also interesting is the extension of the method to a true space-time parallel algorithm, using variants of the cyclic reduction methodology as examined, for example, in [14], to parallelize the solves within waveform relaxation. This would allow a fair comparison between the method investigated herein and standard parallel-in-space timestepping in the common paradigm where there are many more cores available than can be effectively used when strong scaling a fixed spatial problem. Finally, we note that the use of monolithic space-time discretizations, as considered here, allows the possibility of both local-in-space and local-in-time adaptivity, and that extensions of waveform relaxation multigrid (and other efficient monolithic solvers) to this paradigm, where classical timestepping is not directly feasible, would be of great interest.

REFERENCES

- [1] R. ABU-LABDEH, S. MACLACHLAN, AND P. FARRELL, *Monolithic multigrid for implicit Runge-Kutta discretizations of incompressible fluid flow*, *J. Comp. Phys.*, 478 (2023), p. 111961.
- [2] S. BALAY, S. ABHYANKAR, M. F. ADAMS, S. BENSON, J. BROWN, P. BRUNE, K. BUSCHELMAN, E. CONSTANTINESCU, L. DALCIN, A. DENER, V. EIJKHOUT, J. FAIBUSSOWITSCH, W. D. GROPP, V. HAPLA, T. ISAAC, P. JOLIVET, D. KARPEEV, D. KAUSHIK, M. G. KNEPLEY, F. KONG, S. KRUGER, D. A. MAY, L. C. MCINNES, R. T. MILLS, L. MITCHELL, T. MUNSON, J. E. ROMAN, K. RUPP, P. SANAN, J. SARICH, B. F. SMITH, S. ZAMPINI, H. ZHANG, H. ZHANG, AND J. ZHANG, *PETSc/TAO users manual*, Tech. Report ANL-21/39 - Revision 3.21, Argonne National Laboratory, 2024, <https://doi.org/10.2172/2205494>.
- [3] G.-T. BERCEA, A. T. T. MCRAE, D. A. HAM, L. MITCHELL, F. RATHGEBER, L. NARDI, F. LUPORINI, AND P. H. J. KELLY, *A structure-exploiting numbering algorithm for finite elements on extruded meshes, and its performance evaluation in Firedrake*, *Geoscientific Model Development*, 9 (2016), pp. 3803–3815, <https://doi.org/10.5194/gmd-9-3803-2016>.
- [4] M. BJØRHHUS, *On Domain Decomposition, Subdomain Iteration and Waveform Relaxation*, PhD thesis, Department of Mathematical Sciences, Norwegian Institute of Technology, University of Trondheim, Trondheim, Norway, 1995.
- [5] J. D. BOZEMAN AND C. DALTON, *Numerical study of viscous flow in a cavity*, *Journal of Computational Physics*, 12 (1973), pp. 348–363, [https://doi.org/10.1016/0021-9991\(73\)90157-5](https://doi.org/10.1016/0021-9991(73)90157-5).
- [6] A. BRANDT, *Multi-level adaptive finite element methods. 1: Variational problems*, Tech. Report ICASE Report No. 79-8, 1979.
- [7] O. R. BURGGRAF, *Analytical and numerical studies of the structure of steady separated flows*, *Journal of Fluid Mechanics*, 24 (1966), pp. 113–151, <https://doi.org/10.1017/s0022112066000545>.
- [8] A. J. CHORIN, *Numerical solution of the Navier-Stokes equations*, *Mathematics of Computation*, 22 (1968), pp. 745–762, <https://doi.org/10.1090/s0025-5718-1968-0242392-2>.
- [9] F. DANIELI AND S. MACLACHLAN, *Multigrid reduction in time for non-linear hyperbolic equations*, *Electronic Transactions on Numerical Analysis*, 58 (2023), pp. 43–65, https://doi.org/10.1553/etna_vol158s43.
- [10] H. DE STERCK, R. FALGOUT, S. FRIEDHOFF, O. KRZYSIK, AND S. MACLACHLAN, *Optimizing MGRIT and Parareal coarse-grid operators for linear advection*, *Numer. Linear Alg. Appl.*, 28 (2021), p. e2367.
- [11] S. C. EISENSTAT AND H. F. WALKER, *Choosing the forcing terms in an inexact Newton method*, *SIAM Journal on Scientific Computing*, 17 (1996), pp. 16–32.
- [12] D. J. ESTEP AND A. M. STUART, *The dynamical behavior of the discontinuous Galerkin method and related difference schemes*, *Math. Comp.*, 71 (2002), pp. 1075–1103, <https://doi.org/10.1090/S0025-5718-01-01364-3>.
- [13] R. FALGOUT, S. FRIEDHOFF, T. KOLEV, S. MACLACHLAN, AND J. SCHRODER, *Parallel time integration with multigrid*, *SIAM J. Sci. Comput.*, 36 (2014), pp. C635–C661.
- [14] R. FALGOUT, S. FRIEDHOFF, T. KOLEV, S. MACLACHLAN, J. SCHRODER, AND S. VANDEWALLE, *Multigrid methods with space-time concurrency*, *Comput. Vis. Sci.*, 18 (2017), pp. 123–143.
- [15] P. E. FARRELL, M. G. KNEPLEY, L. MITCHELL, AND F. WECHSUNG, *PCPATCH: Software for the topological construction of multigrid relaxation methods*, *ACM Transactions on Mathematical Software*, 47 (2021), pp. 1–22.
- [16] P. FISCHER, S. KERKEMEIER, M. MIN, Y.-H. LAN, M. PHILLIPS, T. RATHNAYAKE, E. MERZARI, A. TOMBOULIDES, A. KARAKUS, N. CHALMERS, ET AL., *NekRS, a GPU-accelerated spectral element Navier–Stokes solver*, *Parallel Computing*, 114 (2022), p. 102982.
- [17] M. J. GANDER, *50 years of time parallel time integration*, in *Multiple Shooting and Time Domain Decomposition Methods*, T. Carraro, M. Geiger, S. Körkel, and R. Rannacher, eds., Cham, 2015, Springer International Publishing, pp. 69–113.
- [18] M. J. GANDER, J. LIU, S.-L. WU, X. YUE, AND T. ZHOU, *Paradiag: Parallel-in-time algorithms based on the diagonalization technique*, arXiv preprint arXiv:2005.09158, (2020).
- [19] W. HACKBUSCH, *Parabolic multigrid methods*, in *Computing methods in applied sciences and engineering*, VI (Versailles, 1983), North-Holland, Amsterdam, 1984, pp. 189–197.
- [20] E. HAIRER AND G. WANNER, *Solving ordinary differential equations. II*, vol. 14 of Springer Series in Computational Mathematics, Springer-Verlag, Berlin, revised ed., 2010, <https://doi.org/10.1007/978-3-642-05221-7>.
- [21] D. A. HAM, P. H. J. KELLY, L. MITCHELL, C. J. COTTER, R. C. KIRBY, K. SAGIYAMA, N. BOUZIANI, S. VORDERWUELBECKE, T. J. GREGORY, J. BETTERIDGE, D. R. SHAPERO, R. W. NIXON-HILL, C. J. WARD, P. E. FARRELL, P. D. BRUBECK, I. MARSDEN, T. H. GIBSON, M. HOMOLYA, T. SUN, A. T. T. MCRAE, F. LUPORINI, A. GREGORY, M. LANGE, S. W. FUNKE,

- F. RATHGEBER, G.-T. BERCEA, AND G. R. MARKALL, *Firedrake User Manual*, Imperial College London and University of Oxford and Baylor University and University of Washington, first edition ed., 5 2023, <https://doi.org/10.25561/104839>.
- [22] F. H. HARLOW AND J. E. WELCH, *Numerical calculation of time-dependent viscous incompressible flow of fluid with free surface*, *Physics of Fluids*, 8 (1965), pp. 2182–2189.
- [23] G. M. HULBERT AND T. J. HUGHES, *Space-time finite element methods for second-order hyperbolic equations*, *Computer Methods in Applied Mechanics and Engineering*, 84 (1990), pp. 327–348, [https://doi.org/10.1016/0045-7825\(90\)90082-w](https://doi.org/10.1016/0045-7825(90)90082-w).
- [24] J. JACKAMAN AND S. MACLACHLAN, *Implementation of experiments in ‘Space-time waveform relaxation for Navier-Stokes’*. Zenodo, jul 2024, <https://doi.org/10.5281/zenodo.12666474>.
- [25] J. JANSSEN AND S. VANDEWALLE, *Multigrid waveform relaxation on spatial finite element meshes*, in *Contributions to multigrid* (Amsterdam, 1993), vol. 103 of CWI Tract, Math. Centrum Centrum Wisk. Inform., Amsterdam, 1994, pp. 75–86.
- [26] J. JANSSEN AND S. VANDEWALLE, *Multigrid waveform relaxation of spatial finite element meshes: the continuous-time case*, *SIAM J. Numer. Anal.*, 33 (1996), pp. 456–474.
- [27] J. JANSSEN AND S. VANDEWALLE, *Multigrid waveform relaxation on spatial finite element meshes: the discrete-time case*, *SIAM J. Sci. Comput.*, 17 (1996), pp. 133–155.
- [28] V. JOHN, A. LINKE, C. MERDON, M. NEILAN, AND L. G. REBHOLZ, *On the divergence constraint in mixed finite element methods for incompressible flows*, *SIAM Review*, 59 (2017), pp. 492–544, <https://doi.org/10.1137/15M1047696>.
- [29] M. LANGE, L. MITCHELL, M. G. KNEPLEY, AND G. J. GORMAN, *Efficient mesh management in Firedrake using PETSc DMPLex*, *SIAM Journal on Scientific Computing*, 38 (2016), pp. S143–S155, <https://doi.org/10.1137/15M1026092>.
- [30] E. LELARASMEE, A. E. RUEHLI, AND A. L. SANGIOVANNI-VINCENTELLI, *The waveform relaxation method for time-domain analysis of large scale integrated circuits*, *IEEE CAD*, 1 (1982).
- [31] J. L. LIONS, Y. MADAY, AND G. TURINICI, *Résolution d’EDP par un schéma en temps parallèle*, *C.R.Acad Sci. Paris Sér. I Math*, 332 (2001), pp. 661–668.
- [32] C. LUBICH AND A. OSTERMANN, *Multigrid dynamic iteration for parabolic equations*, *BIT*, 27 (1987), pp. 216–234.
- [33] A. MOIOLA AND I. PERUGIA, *A space-time Trefftz discontinuous Galerkin method for the acoustic wave equation in first-order formulation*, *Numerische Mathematik*, 138 (2017), pp. 389–435, <https://doi.org/10.1007/s00211-017-0910-x>.
- [34] N. OFFERMANS, O. MARIN, M. SCHANEN, J. GONG, P. FISCHER, P. SCHLATTER, A. OBABKO, A. PEPLINSKI, M. HUTCHINSON, AND E. MERZARI, *On the strong scaling of the spectral element solver Nek5000 on petascale systems*, in *Proceedings of the Exascale Applications and Software Conference 2016, EASC ’16*, New York, NY, USA, 2016, Association for Computing Machinery, <https://doi.org/10.1145/2938615.2938617>.
- [35] C. W. OOSTERLEE AND P. WESSELING, *Multigrid schemes for time-dependent incompressible Navier-Stokes equations*, *Impact Comput. Sci. Engrg.*, 5 (1993), pp. 153–175.
- [36] L. F. PAVARINO, *Additive Schwarz methods for the p-version finite element method*, *Numerische Mathematik*, 66 (1993), pp. 493–515, <https://doi.org/10.1007/BF01385709>.
- [37] A. RAFIEI AND S. MACLACHLAN, *Improved monolithic multigrid methods for high-order Taylor-Hood discretizations*, (2024). In preparation.
- [38] O. STEINBACH, *Space-time finite element methods for parabolic problems*, *Computational Methods in Applied Mathematics*, 15 (2015), pp. 551–566, <https://doi.org/10.1515/cmam-2015-0026>.
- [39] J. VAN LENT AND S. VANDEWALLE, *Multigrid waveform relaxation for anisotropic partial differential equations*, *Numer. Algorithms*, 31 (2002), pp. 361–380.
- [40] S. VANDEWALLE AND G. HORTON, *Fourier mode analysis of the multigrid waveform relaxation and time-parallel multigrid methods*, *Computing*, 54 (1995), pp. 317–330.
- [41] S. G. VANDEWALLE AND E. F. VAN DE VELDE, *Space-time concurrent multigrid waveform relaxation*, *Ann. Numer. Math.*, 1 (1994), pp. 347–360. *Scientific computation and differential equations* (Auckland, 1993).
- [42] E. VAROĞLU AND W. D. LIAM FINN, *Space-time finite elements incorporating characteristics for the Burgers’ equation*, *International Journal for Numerical Methods in Engineering*, 16 (1980), pp. 171–184, <https://doi.org/10.1002/nme.1620160112>.
- [43] *Software used in ‘Space-time waveform relaxation multigrid for Navier-Stokes’*, jul 2024, <https://doi.org/10.5281/zenodo.12657473>.

JAMES JACKAMAN DEPARTMENT OF MATHEMATICAL SCIENCES, NTNU, 7491 TRONDHEIM, NORWAY james.jackaman@ntnu.no.

SCOTT MACLACHLAN DEPARTMENT OF MATHEMATICS AND STATISTICS, MEMORIAL UNIVERSITY OF NEWFOUNDLAND, ST. JOHN’S, NL, A1C 5S7, CANADA smaclachlan@mun.ca.